A Robotic Surgery Platform for Automated Tissue Micromanipulation in Zebrafish Embryos

Ece Özelçi, Erfan Etesami, Laurel A. Rohde, Andrew C. Oates, and Mahmut Selman Sakar

***Abstract*—Microsurgical manipulations are key experimental techniques in life science research, particularly in embryology. These techniques are most often performed manually by highly skilled scientists, posing limitations on speed, precision, and reproducibility. Here we introduce a fully automated robotic microsurgery platform that generates explants of specific tail tissue from growing zebrafish embryos, a popular model organism for vertebrate development. Our work leverages both classical and deep learning-based image-processing techniques to perform robotic micromanipulation on biological specimens. Using two example experimental cases as proof of concept, we show that our automated platform is more precise, accurate, and efficient than teleoperated and manual microsurgery conducted by experienced scientists. Moreover, we demonstrate the usefulness of our platform for inexperienced experimentalists, supporting an important role for robotic microsurgery in broadening the use of such techniques in experimental research.**

***Index Terms*—Automation at micro-nano scales, computer vision for automation, microsurgery, zebrafish embryos.**

I. Introduction

MICROSURGERY is a discipline that combines specialized precision instruments and magnification with advanced microscopy to operate on small and delicate tissues [1]. Beyond an essential role in medicine, precise surgical manipulations are a fundamental component of experimental work in many life sciences domains, particularly embryology, neuroscience, and translational research. A classic example is the Nobel prize-winning work of Hans Spemann and Hilde Mangold (1935) in which they explanted tissue from one embryo and then transplanted it into a second to demonstrate the existence of embryonic organizer tissue [2]. Most microsurgeries on lab-grown tissues or model organisms are still performed manually, using basic tools such as razor blades, microknives, forceps, scissors, and glass capillaries [3], [4]. On top of requiring steady hands and often years of training, these manual techniques are difficult to standardize and are limited in speed, precision, and accuracy. Here we address these challenges by developing a fully-automated microsurgical platform designed for research using zebrafish embryos.

We decided to target our platform to zebrafish because it is a widely-used model system for studying vertebrate development due to shared genetics and developmental programs with humans [5], [6]. Zebrafish embryos are particularly suited for microsurgical approaches because of their rapid external development and tissue transparency that allows internal structures and fluorescent proteins to be visualized in the growing embryo [6]. Microsurgical approaches in experiments on zebrafish embryos are common and include injection, cell transplantation, tissue ablation, and generation of explants [7], [8], [9]. Previously, we showed the feasibility of generating tail explants from zebrafish embryos using a robotic microsurgery platform that was teleoperated by a scientist observing through a stereomicroscope (Fig. 1(a)) [10].

Our scientific aim is to study the mechanics of body axis morphogenesis and segmentation. As vertebrate embryos elongate, tissue blocks called somites successively form with rhythmic timing from the presomitic mesoderm (PSM) in the trunk and tail (Fig. 1(b)). Our teleoperated platform was critical to dissecting the dynamic interplay between somite formation and tissue mechanics, which are thought to include flow, deformation, and phase transitions [7], [11], [12], [13], by enabling precise micromanipulation of embryonic tissue and the generation of tail explants. This success was consistent with the known power of robotic microsurgery platforms to increase reproducibility, precision, and throughput, as well as reduced tissue damage [14], [15], [16], [17].

Going to the next step of fully automated microsurgery has the potential to extend the usability of our platform to the wider research community by eliminating the need for highly-trained experimentalists [15], [18], [19], [20]. Notably, automation contributes to the reduction of tissue damage in microsurgical procedures. Pioneering work has shown that operating on

Manuscript received 11 June 2023; accepted 9 November 2023. Date of publication 16 November 2023; date of current version 24 November 2023. This letter was recommended for publication by Associate Editor T. Xu and Editor X. Liu upon evaluation of the reviewers' comments. This work was supported by the EPFL School of Life Sciences iPhD Program. *(Corresponding author: Mahmut Selman Sakar.)*

This work involved human subjects or animals in its research. Approval of all ethical and experimental procedures and protocols was granted by the Service de la Consommation et des Affaires Vétérinaires of canton Vaud, Switzerland under Application No. VD-H23.

Ece Özelçi and Mahmut Selman Sakar are with the Institute of Mechanical Engineering, Ecole Polytechnique Fédérale de Lausanne (EPFL), CH-1015 Lausanne, Switzerland, and also with the Institute of Bioengineering, EPFL, CH-1015 Lausanne, Switzerland (e-mail: ece.ozelci@epfl.ch; selman.sakar@epfl.ch).

Erfan Etesami is with the Institute of Mechanical Engineering, Ecole Polytechnique Fédérale de Lausanne (EPFL), CH-1015 Lausanne, Switzerland (e-mail: erfan.etesami@epfl.ch).

Laurel A. Rohde and Andrew C. Oates are with the Institute of Bioengineering, EPFL, CH-1015 Lausanne, Switzerland (e-mail: laurel.rohde@epfl.ch; andrew.oates@epfl.ch).

This letter has supplementary downloadable material available at https://doi.org/10.1109/LRA.2023.3333690, provided by the authors.

Digital Object Identifier 10.1109/LRA.2023.3333690

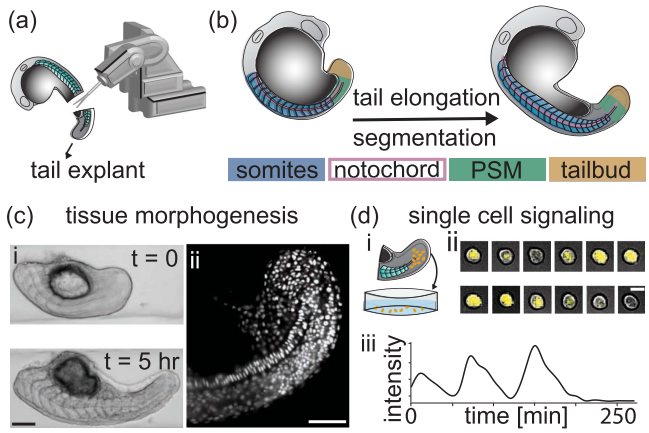

Fig. 1. Robotic microsurgery for embryology. (a) Schematic of tail explant generation with robotic microsurgery. (b) Schematic of zebrafish embryo at two different developmental stages. Relevant tissues are highlighted with different colors. PSM is the acronym for the presomitic mesoderm. (c) Using explants to study morphogenesis of body axis elongation and growth. i. A bright-field image of an explant right after dissection and after 5 hours of culture. ii. Light-sheet fluorescence image of an explant expressing fluorescently-tagged histone transgene for nuclear marking. Scale bars, 100 μm. (d) Using explants to study single-cell behavior. i. Schematic for the process of isolating single cells from tail explants. ii. Time-lapse images of Her1-YFP signal from a single isolated cell (from top left to bottom right). iii. Representative plot showing the oscillatory behavior of gene expression. The vertical axis is the intensity of Her1-YFP signal in arbitrary units. Scale bar, 10 μm.

mice using an automated cranial microsurgery platform significantly improves performance, providing access for a wide range of researchers to advanced neurotechnologies [21]. In addition to neurosurgery, ophthalmic surgeries also require extreme precision. Robot assistance has been successfully implemented in various forms including telemanipulation and co-manipulation [22], [23]. Recently, fully automated robotic microsurgery has been demonstrated in posterior ocular procedures. The robotic system automatically removes exceptionally thin membranes without causing damage to the surrounding tissues — a challenging task even for highly skilled clinicians [24].

The motivation for building a robotic microsurgeon for embryonic research comes from our success at using tail explants grown in culture as a testbed to explore how specific tissues drive morphogenesis (Fig. 1(c)). Moreover, it has previously been shown that individual cells can be isolated from dissociated PSM explants to study the autonomous dynamics of gene expression in segmentation (Fig. 1(d)) [25]. Considering the rapid advances in various single-cell technologies such as genomics, proteomics, and metabolomics, we believe that robotic microsurgery to generate large numbers of cells from precise explants taken from embryos or organoids will be more widely adopted.

Here, we present several advancements toward fully automated tissue micromanipulation in zebrafish embryos. We developed a controller that communicates with several peripheral instruments to autonomously detect distinct features of embryos placed in a microwell array, then drives microscissors mounted on a 6-DOF robot to cut out the desired part of the tail. We designed two representative case studies. The first case study involved explanting unsegmented tissue at a single developmental time point from a group of embryos that were at the same developmental stage. The second case study also used the robot to generate explants in a group of embryos, however, the challenge was to repeat this at multiple time points as the embryos develop. In the first case, we devised an algorithm based on classical computer vision functions. This approach was computationally light and did not require the collection and annotation of a dataset. However, adapting this algorithm to identify tissue targets on embryos at different developmental stages in the second case proved to be inefficient, thus we opted for a more versatile detection algorithm based on machine learning. When trained properly, the algorithm successfully guided the robot to generate explants from embryos of varying sizes and shapes throughout development. Compared to manual and teleoperated microsurgery, we found that automation reduced the duration of the microsurgery while increasing accuracy and precision. Our results illustrate the potential contributions of automated microsurgery to embryology research in zebrafish and other model organisms.

II. System Overview

The automated robotic microsurgery platform we designed consists of a motorized stage that translates and rotates the specimen, and a surgery microrobot that moves and actuates microscissors. We chose microscissors (Advanced DSP Tip 27+ Straight Scissors, 727.53, Alcon) as the surgical instrument because microscissors have short, fine blades that provide visibility and precision in confined places, facilitating the sharp dissection of delicate embryos. The stage has a two-axis linear positioner (PI, VT-80 100-DC) with a 10 cm travel range and 0.5 μm resolution, and a rotary positioner (PI, U-651.04 V) to align the specimen with respect to the microscissors (Fig. 2(a)). The rotary positioner is attached to the linear positioners with 3D-printed parts.

The body of the microrobot is equipped with a motorized 6-DOF micromanipulator (SmarAct Gmbh) capable of moving the microscissors (i.e., the end effector) with 4 nm translation and 25 μ^o rotation resolution. The movement is performed with three translational positioners (X, Y, Z), two rotary positioners (roll, α, and pitch, β), and an open-loop light-weight rotary positioner (yaw, γ) mounted on the adapter enabling continuous axial rotation of the end-effector (Fig. 2(b)). An aluminum adapter, designed and micromachined to hold the microscissors, is directly mounted on the β positioner. The back-and-forth movement of a plunger against a passive spring-loaded mechanism controls the opening and closing of the microscissors' blades (Fig. 2(b)). The lead screw on the stepper motor acts as a piston to push the plunger.

A compact stepper motor (Haydon Kerk, LC15AQ12) is mounted on the adapter piece with the tubular motor support to actuate the end-effector. The motor is controlled by an Arduino connected to a stepper motor driver (Easy drive, V4.4). An Xbox One gamepad with customized button control settings

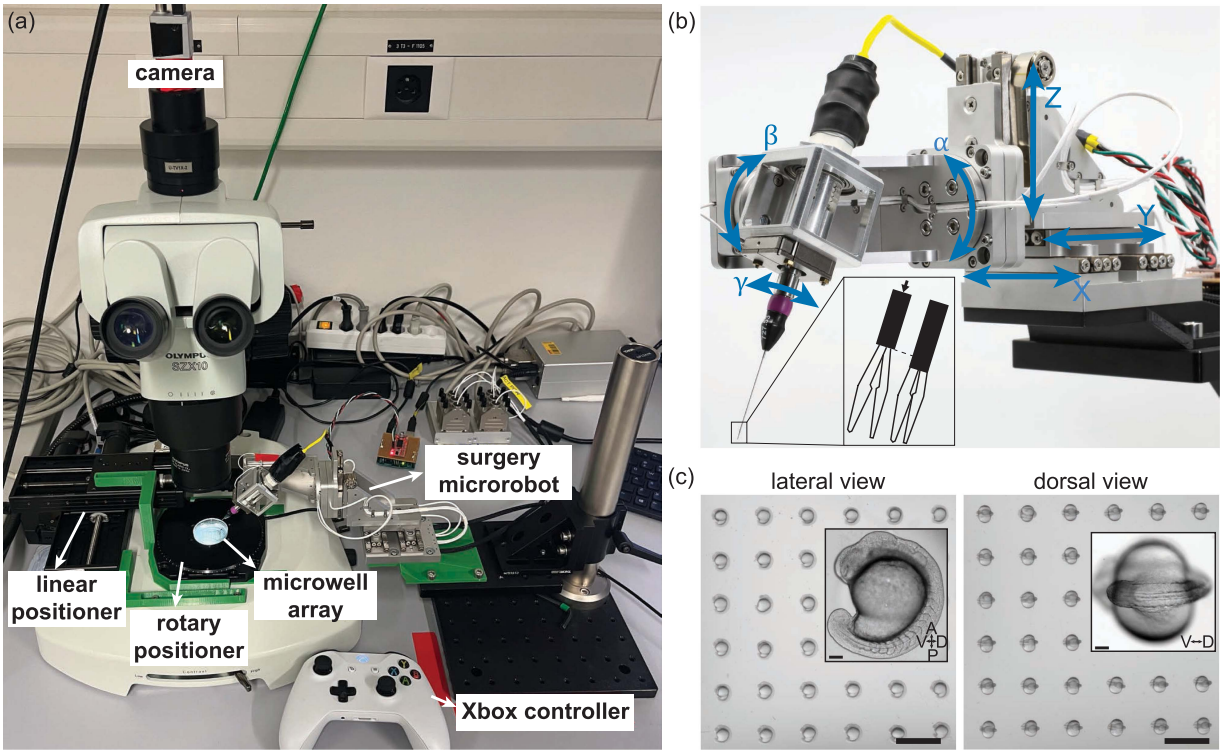

Fig. 2. Automated robotic microsurgery platform. (a) An image of the platform highlighting the major components. (b) The 6 degrees of freedom of the surgery microrobot. The schematic illustrates the actuation mechanism of the microscissors. (c) Microscope image of the microwell array showing the embryos placed along their lateral and dorsal axes. Scale bars, 2 mm. Insets display enlarged lateral and dorsal views of a 15-somite-stage zebrafish embryo. The diameter of a single well is 600 μm. Scale bars, 100 μm. (A/P: anterior/posterior. D/V: dorsal/ventral).

serves as the human-machine interface for the teleoperation of the system. A CCD camera (Basler, acA1920-155uc) mounted on a stereomicroscope (Olympus SZX10) allows observation of the specimen and provides visual feedback. Agarose microwell arrays were fabricated from 3D-printed ABS-tough molds to facilitate the imaging and surgical manipulation of the embryos (Fig. 2(c)). The microwell array resides on the rotary positioner.

III. Software Architecture

Fig. 3(a) illustrates the software architecture, summarizing the various connections among the cyber and physical components of the platform. The code was developed in Python with C++ scripts that interface with the driver of the microsurgery robot. Both positioners and the motorized micromanipulators of the surgery microrobot are controlled by PID controllers based on the visual feedback provided by computer vision. The framework is initialized with hardware adjustments including referencing and positioning. Once initialization is completed, the user activates the camera for image acquisition. In the automated surgery mode, external Python libraries perform computer vision to detect the key locations on the embryo and the end effector. The coordinates extracted from the processed images are transferred to the controller of the 6-DOF surgery microrobot, which drives the positioners. When the robot is ready to perform surgery, the relevant script is activated to turn on the stepper motor and actuate the end-effector. After each surgical operation, a predefined trajectory array drives the linear positioners to bring the next embryo. The control loop restarts once the linear positioners bring the next embryo in the microwell array to the workspace. The control architecture of the system explaining these steps is shown in Fig. 3(b).

The high-level programming interface has two main blocks: (1) the graphical user interface (GUI) and (2) worker threads (Fig. 3(a)). We developed the GUI using Python modules *PyQt5* and *PyQtGraph*. The GUI controls all the peripheral devices and operation modes. Running background tasks and simultaneous actions may cause problems during application updates. To ensure that the GUI does not freeze during these updates, we implemented a multi-threading approach using separate worker threads, allowing control of all components in parallel.

Each gamepad axis and button of the Xbox controller was assigned to a specific feature of the hardware components with the "gamepad" class in Python. We also wrote an "ASM" (Arduino Stepper Motor) class using the *PySerial* library to control the stepper motor. The images acquired by the CCD camera were exported with the *pypylon* library. Importantly, the GUI is user-friendly, where the different action sequences can be easily modified on the screen and requires no coding experience. The software can be accessed from the following GitHub repository.[1]

[1][Online]. Available: https://github.com/ecominator/robotic_microsurgery_automation.git.

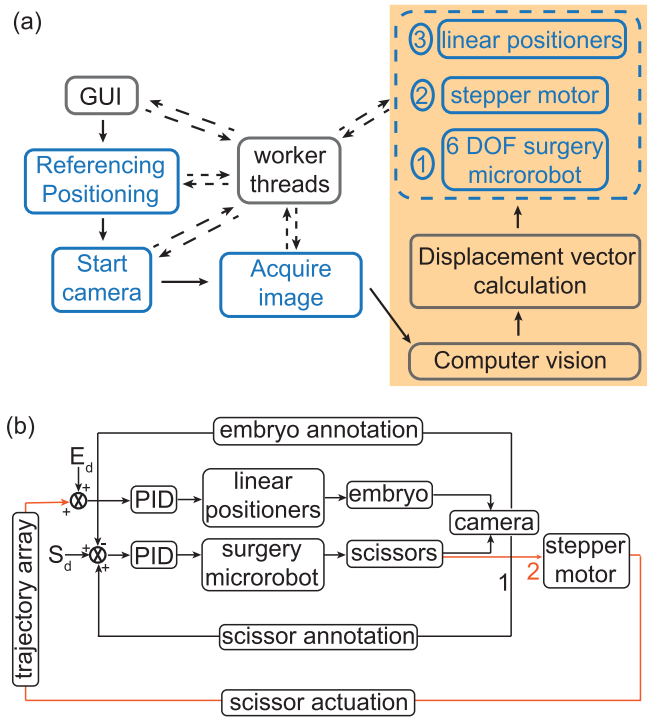

Fig. 3. Software architecture. (a) High-level programming interface of the control software for the robotic microsurgery platform. Blue and black components refer to hardware and software-based actions respectively. Dashed arrows are to indicate the worker thread connections. Continuous arrows show the work sequence starting from the GUI. The shaded area indicates the operations performed for a single embryo. (b) System control architecture. "E_d" and "S_d" refer to the desired initial positions of the embryo and the scissors, respectively. "1" and "2" refer to the first action (the annotation of the microscissors) and the second action (the actuation of the microscissors which then triggers the movement of the linear positioners that carry the embryos) of the surgery microrobot.

IV. Results and Discussion

As a proof of principle for our fully automated platform, we designed two experimental case studies based on ongoing research work (Fig. 1) that relies on generating tail explants from precise locations and developmental stages of zebrafish embryos. The chorion of the zebrafish embryos was surgically removed using two forceps (FST-Dumont #5, 91150-20) (Video 1). The released embryos were transferred using a glass Pasteur pipette and placed inside agarose microwells with the dorsal side facing up. These operations were done manually by the researcher. After the manual placement of the embryos, the automated dissection process was initiated to control stage movement, visual servoing of the surgery microrobot, and actuation of the microscissors. During the experiments, linear positioners were programmed to move at a constant speed of 1 mm·s^{-1}, and the maximum speed for the translational positioners of the micromanipulator was set at 1.5 mm·s^{-1} to maintain the orientation of the embryos inside the microwells and to avoid damaging the embryos, respectively.

Case Study 1: The objective of the first study was to rapidly, precisely, and accurately generate tail explants by cutting directly posterior to the last formed somite in multiple embryos at the same developmental stage (see Video 2). High throughput can often be difficult to achieve using slow-paced manual dissection due to the rapid development of the embryo. Embryos at the 15-somite stage were placed in the microwell array and positioned dorsal side up. Because the orientation of the embryos was the same and the ambient illumination conditions were stable, we used conventional image processing techniques to detect key features of both the embryos and microscissors. An algorithm implemented using the OpenCV module of Python detected the key features of the embryo, which were then used to calculate the distance between the target tissue and the microscissors. The x- and y-axis of the surgery microrobot was then instructed to move such that the microscissors were positioned at the desired location. Finally, the positioner controlling the z-axis of the robot was activated to translate the microscissors down. The precise displacement in the z-axis was determined through an initial calibration measurement conducted on a single embryo for each microwell array. The same displacement was used to operate on all the embryos in an array as the embryos were at the same developmental stage. The initial calibration is critical because although we consistently cast a constant volume of liquid agarose gel (2 ml for 35mm-Mattek petri dish) there is a small variation in the height of the agarose molds.

The image processing framework performed the following steps: (1) the acquired image was blurred to remove the noise; (2) thresholding was applied to the blurred image to distinguish the embryo and the microscissors as separate objects; (3) parameters were manually tuned once and applied to all the subsequent surgeries; (4) parts of the images corresponding to the embryo and microscissors were cropped for further processing; (5) image processing techniques that involved closing, filling, and edge detection (Canny edge detector) were used to identify the contour of the embryo, from which the centroids of the relevant locations (i.e., top and bottom sides of the notochord) were calculated; (6) closing, filling, and line detection (probabilistic Hough transform) identified the intersection point of the scissors' blades; and (7) the detected points were projected on the acquired image as shown in Fig. 4(a). We found this image-processing framework to be robust and computationally light, with an execution time of 180 milliseconds per embryo.

To evaluate the advantages of automation in this case study, we compared the duration of automated robotic microsurgery to that of robot-assisted microsurgery in which the robot was teleoperated, and manual microsurgery. All work, in this case, was done by a scientist who had 4 years of experience with zebrafish micromanipulation. Each microwell array contained 36 embryos, which were operated on in a single run for speed measurements. First, we evaluated how fast the microsurgeries could be done with the different methods. The average time for dissecting one embryo with automated, teleoperated, and manual microsurgery was 19.4 ± 0.6 (N = 4, n = 144), 35.2 ± 3.5 (N = 3, n = 108), and 37.2 ± 2.5 (N = 3, n = 108) seconds, respectively (Fig. 4(b)) (N = the number of individual experimental runs, n = the total number of embryos undergoing microsurgery). We found that automated microsurgery was twice as fast on average than the other methods, with a smaller inter-experiment standard deviation, indicating that automated dissection is both faster and more precise. Because a new somite forms on average every

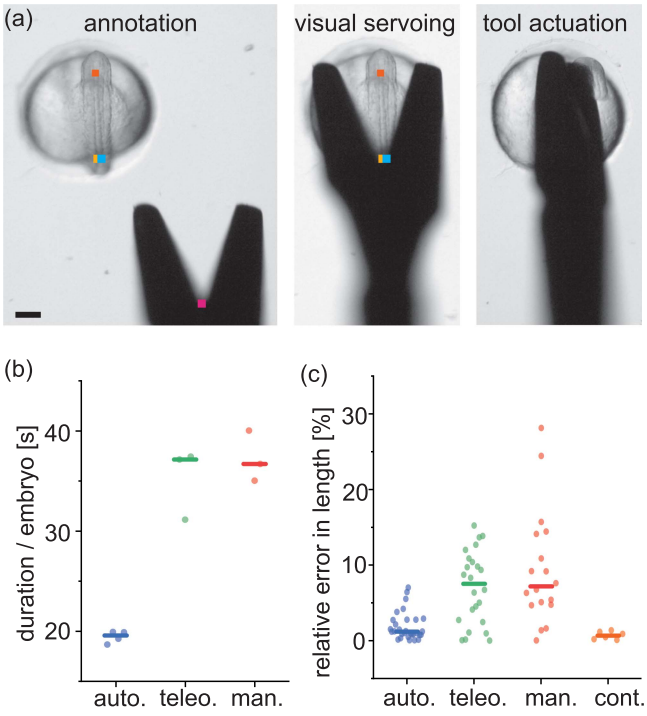

Fig. 4. High throughput dissection of tail explants. (a) The sequence showing automated microsurgery steps. Yellow and orange squares indicate the centroid of the lower part and upper part, respectively, and blue square indicates the mean of the x-components of the upper and lower centroids. Pink square is the target location on the microscissors. Scale bar, 100 μm. (b) The duration of explant generation per embryo done with automated, teleoperated, or manual microsurgery. (c) The percent error in the length of the explant for automated, teleoperated, or manual microsurgery. Lines indicate the median.

30 min (at 28.5 °C) during segmentation of the embryo [26], an experimenter would be restricted to a 30 min window in which to collect explants at the same developmental stage. Using the speeds determined here, we anticipate that full automation would enable 93 explants to be collected within this window, as opposed to 51 for teleoperation and 48 for manual operation, thus meeting our objective of improving high throughput sample collection.

Next, we wanted to see if this increase in throughput through automation was accompanied by an increase in the accuracy of placement of the cut to generate the explants. To facilitate analysis, we performed these surgeries on 6 embryos per round, following four steps: (1) embryos were oriented laterally and a picture of each embryo was taken, (2) embryos were then positioned dorsally for microsurgery, (3) microsurgery was used to generate explants, and (4) explants were oriented laterally and imaged. We measured the length of the tail of the intact embryo before surgery, l_{intact}, and the length of the explant post-surgery, $l_{explant}$, to quantify the relative error, which is given by $(l_{intact} - l_{explant}) \times 100/l_{intact}$. To control for measurement variability, we measured the length of the tail in an intact embryo at the start and finish of the microsurgery interval. The computed relative error for the control case was 0.69 $\pm$ 0.52 % (N = 6, n = 6), which we attributed to measurement errors. The

TABLE I
INEXPERIENCED USERS' PERFORMANCE DURING MANUAL AND TELEOPERATED SURGERIES

user #	operation	# surgeries in 30 min	# viable explants
1	manual	36	9
	teleoperation	16	13
2	manual	32	11
	teleoperation	34	32
3	manual	8	4
	teleoperation	16	16

computed relative error of the automated procedure was 1.87 $\pm$ 1.86 % (N = 6, n = 30), which was significantly lower than both teleoperation (7.01 $\pm$ 4.84 %, N = 4, n = 24) and manual surgery (9.40 $\pm$ 7.57 %, N = 3, n = 18) (Fig. 4(c)). Thus, automated robotic microsurgery was 3 times more accurate than the other methods. Once again, we calculated a smaller standard deviation from the robotic microsurgery data, highlighting the precision brought by automation.

To determine if automation, in this case, makes microsurgery accessible to untrained experimentalists, we asked three researchers who had no prior experience with zebrafish embryos and our robotic platform to generate explants. Performances of the different operators during manual surgery greatly varied, but in all cases, the addition of robotic assistance via teleoperation significantly improved the precision and accuracy of viable dissections. Overall, automation of the surgery was 10 to 20 times faster than manual surgery, and 3 to 7 times faster than teleoperated surgery. Importantly, full automation enables an inexperienced user to collect the same number of explants at a single somite stage as an experienced user, whereas with teleoperation or manual techniques only 13–32 or 4–11 explants were generated within a 30 min window, respectively (Table I).

Taken together, these results show that automation outperforms robot-assisted and manual microsurgeries in terms of speed, accuracy, and precision, and has the potential to make these experiments possible for inexperienced experimentalists.

Case Study 2: The objective of the second study was to generate explants of unsegmented tissue at successive developmental stages (see Video 3). To achieve this, we let the embryos grow inside the microwell array and cut their tails at multiple time points pre-defined by the user (Fig. 5(a)). In addition to speed and accuracy, automation is useful for this type of dynamic manipulation that would otherwise require the scientist to be present throughout the entire developmental window.

Because embryos morph in 3D over time, the classical image processing techniques used in the previous case study were incapable of detecting the features of the embryo. To address this issue, we implemented a deep learning-based solution.

In biomedical image processing, where a limited number of images are available for annotation, Deep Convolutional Neural Networks (DCNNs) excel in tasks such as detection, classification, segmentation, and information processing [27], [28]). Previous work has shown that DCNNs outperform other methods in various visual recognition tasks [27]. We generated a dataset of 210 dorsal view images of zebrafish embryos and annotated

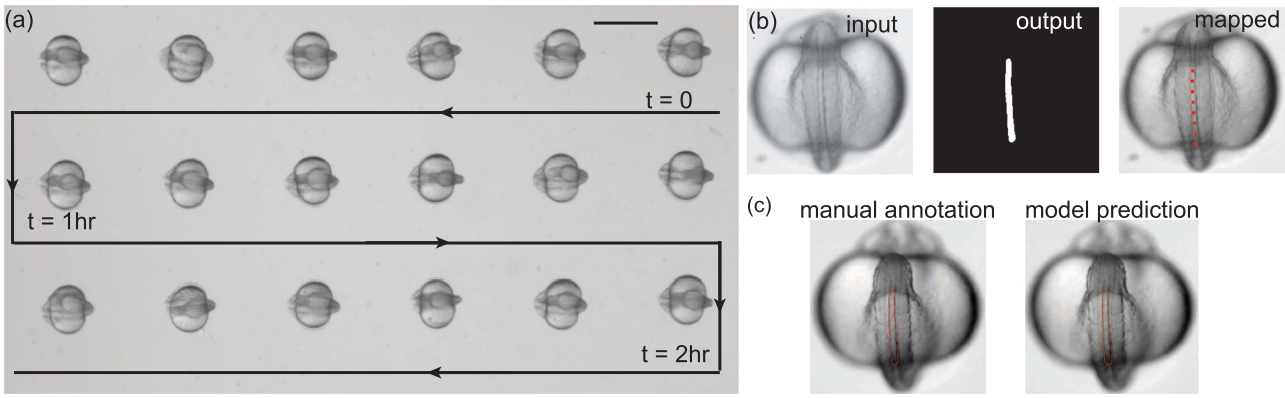

Fig. 5. Automated microsurgery on developing embryos. (a) A representative image of embryos from the same developmental stage placed in the microwell array. Black lines show the trajectory for the movement of the xy-stage. Scale bar, 1 mm. (b) Input image to the adapted u-net model and the output mask tracing the notochord together with the annotated embryo image that is fed back to the GUI for visual servoing. Red points on the embryo correspond to the predicted intervals of the somite boundary. (c) Representative images showing the manually annotated notochord along with the model's prediction. The outline of the annotated and the output masks are used for ease of visualization.

them. To use the available annotated samples more efficiently for image segmentation, we used the u-net model [27], a CNN architecture designed to take advantage of data augmentation. The architecture contains an encoder network with max pooling operators and a decoder network with upsampling operators. Here, the encoder has 2D convolutional blocks with a kernel size of 3×3 and same padding to preserve the image size. Each convolutional layer was followed by a batch-normalization and a rectified linear unit (ReLU) activation function. 2×2 max pooling layers reduce the sensitivity of the network to the spatial location of the features detected by the convolutional layers. To reduce overfitting, each max pooling layer was followed by a dropout layer with a rate of 0.5. The upsampling layers of the decoder have the same kernel size as the convolutional layers, using a stride of 2 along both width and height dimensions. The output of each upsampling layer was concatenated along the channel dimension. After each concatenation, the dropout operation with a rate of 0.5 was applied. Finally, the output layer of the network was a convolutional layer with a 1×1 kernel size. A sigmoid activation function was applied on this output layer to ensure that output values were bounded between zero and one. The final output of the network is a grayscale mask.

Detecting somite boundaries in the dorsal view, the preferred view for surgical dissection, proved a challenging task, particularly in young embryos (before the 15 somite stage). Our initial attempts to create a dataset for semantic segmentation models targeting the somite boundaries were not robust. To address these morphological constraints, we used an alternative approach to segment the tail. Unlike somite boundaries, the notochord is clearly visible in the acquired images, and by tuning the hyperparameters, we trained a u-net model to detect the notochord. The input of the adapted u-net model was a grayscale image of the embryo and the output was a binary image of the notochord (Fig. 5(b)). Because the anteroposterior length of each somite is approximately 50 μm, we were able to divide the detected notochord into somite-length sections by specifying this in the software. We then used the output mask to deliver a set of points along the detected notochord as approximate somite boundary locations and projected these points on the input image (Fig. 5(b), mapped). This was a coherent approximation for different embryos because we started to generate the notochord mask from the same anteroposterior position on the embryo axis during the data set creation. The first marked red point was at an identical location in all embryos, and the remaining points were assigned using the same Euclidean distance.

We trained the network on Google Colab with GPU acceleration and a batch size of 5 for 200 epochs. The best model had a training and validation accuracy of 92.5% and 91.0%, respectively. For comparison, the red contours in Fig. 5(c) show an example of a manually annotated notochord and the model's predicted output. The average execution time during the experiment for this protocol was 0.58 seconds.

We designed an experiment where embryos at the 15 somite stage were placed into the top three rows of the microwell array (Fig. 5(a)). Before we started the experiment, we specified at which target location (red point, (Fig. 5(b))) the cutting should initiate. The robot was programmed to start cutting from the top-right corner of the array, operating on the 6 embryos located in the first row. Then, according to our instructions, the robot waited for 1 hr to let the remaining intact embryos form two new somites, raising the total number of somites to 17, and re-activated the surgery sequence to operate on the next 6 embryos located in the second row. This procedure was repeated once more to dissect explants from embryos with 19 somites located in the third row. Fig. 6 shows close-up images of the zebrafish embryos corresponding to the different time points. After all the explants were dissected, we performed time-lapse imaging every 15 minutes for 2 hours. The results showed that the robot successfully cut the same part of the tail, the distal part containing PSM and the tailbud, from embryos at different developmental stages. Post-surgery, the explants continued to elongate and pattern somites (Fig. 6).

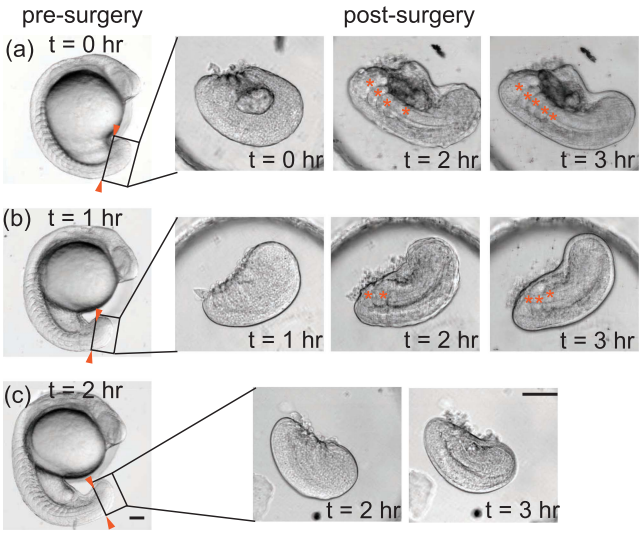

Fig. 6. Explants obtained at multiple time points in developing embryos. Images taken pre-surgery show the zebrafish embryos at the target developmental stages. Orange arrowheads indicate the desired cut location. Six embryos were operated on at each time point (t = 0, 1, 2 hours). Images taken immediately post-surgery show no somite boundaries. Subsequent development includes sequential formation of somite boundaries in the explant. Orange asterisks mark the formed somites. Exemplary images of the embryos operated at time points (a) t = 0, (b) t = 1 hr, and (c) t = 2 hr. Scale bars, 100 μm.

V. Summary and Outlook

In this work, we introduced an automated robotic microsurgery platform for high throughput, precise, and accurate dissection of zebrafish embryos. We specifically designed our platform as a benchtop system that fits adjacent to a conventional microscope and can be operated without programming expertise. Using the hardware details and software provided here, this system can be set up in any research laboratory, making mechanical micromanipulation-based life-sciences applications broadly accessible.

We showed the feasibility of programming a robot to repeatedly generate tissue explants of a specific tail region from a batch of embryos that were the same genotype and developmental stage. Moreover, we designed an improved DCNN-based dynamic protocol to generate explants of a specific tail region at multiple time points throughout development in a single batch of fish. We found that a solution based on OpenCV worked well in the first case, whereas our deep learning-based feature detection method worked better for tasks involving growth and shape change, despite the higher computational cost.

We focused on distinct morphological features, the notochord, and the somites, to generate the tail explants. To this end, we trained the DCNN model to detect the notochord of the embryo and position the microscissors through visual servoing. As an extension of our work, a larger dataset with multi-view images of embryos could be constructed from several developmental stages and other morphological features could be incorporated into the set of labels. This would be a means of programming the microrobot to surgically remove other tissues in the zebrafish embryo, such as the heart, eye, yolk, and nervous system, to grow as explants or to study tissue regeneration [29], [30]. To show the versatility of our platform, we designed a proof-of-concept experiment where the robot was programmed to dissect the head region of the embryo that contains the eye. The robot successfully dissected the targeted tissue using the same image processing functions described in Case Study 1 (see Video 4). Our platform and approach could also be applied to other model organisms, including amphibians, chick, and mouse embryos as well as organoids and other tissue culture models [31], providing endless experimental opportunities for biomedical research.

Here, we focused on automating the microsurgery while handling embryos and explants manually. Our future work will address automating embryo placement into the microwells and collection of explants post-surgery for further culture and analysis, thus automating the entire experimental workflow. Automation also offers new avenues on the imaging side. Recent work has shown the feasibility of using DCNN to classify mutant zebrafish embryos from microscope images [32]. We envision an exciting future in which the robot is programmed to operate on select embryos displaying certain features identified through intelligent imaging and smart microscopy.

V. Acknowledgment

The authors would like to thank Adrien Méry, Clément Helsens, Hannah Trub, and Lorenzo Noseda for participating in the user study, and the members of Oates and MICROBS laboratories as well as David Gonon for their intellectual feedback. The authors also thank the zebrafish facility at EPFL, especially Chloé Jollivet, Florian Lang, and Guillaume Valentin for their assistance with zebrafish husbandry and line maintenance. Permission to do experiments with zebrafish embryos was granted by the Service de la Consommation et des Affaires Vétérinaires of canton Vaud, Switzerland (authorization number VD-H23).

References

[1] D. Zhang, J. Chen, W. Li, D. B. Salinas, and G.-Z. Yang, "A microsurgical robot research platform for robot-assisted microsurgery research and training," *Int. J. Comput. Assist. Radiol. Surg.*, vol. 15, no. 1, pp. 15–25, 2020.

[2] The nobel prize in physiology or medicine 1935. [Online]. Available: https://www.nobelprize.org/prizes/medicine/1935/spemann/facts/

[3] Y. Sasai, M. Eiraku, and H. Suga, "In vitro organogenesis in three dimensions: Self-organising stem cells," *Development*, vol. 139, no. 22, pp. 4111–4121, 2012.

[4] Y. Yang et al., "Heightened potency of human pluripotent stem cell lines created by transient BMP4 exposure," *Proc. Nat. Acad. Sci.*, vol. 112, no. 18, pp. E2337–E2346, 2015.

[5] A. Brownlie et al., "Positional cloning of the zebrafish sauternes gene: A model for congenital sideroblastic anaemia," *Nature Genet.*, vol. 20, no. 3, pp. 244–250, 1998.

[6] T.-Y. Choi, T.-I. Choi, Y.-R. Lee, S.-K. Choe, and C.-H. Kim, "Zebrafish as an animal model for biomedical research," *Exp. Mol. Med.*, vol. 53, no. 3, pp. 310–317, 2021.

[7] A. Mongera et al., "A fluid-to-solid jamming transition underlies vertebrate body axis elongation," *Nature*, vol. 561, no. 7723, pp. 401–405, 2018.

[8] M. Behrndt et al., "Forces driving epithelial spreading in zebrafish gastrulation," *Science*, vol. 338, no. 6104, pp. 257–260, 2012.

[9] M. F. Simsek and E. M. Özbudak, "Spatial fold change of FGF signaling encodes positional information for segmental determination in zebrafish," *Cell Rep.*, vol. 24, no. 1, pp. 66–78, 2018.

[10] E. Özelçi, E. Mailand, M. Rüegg, A. C. Oates, and M. S. Sakar, "Deconstructing body axis morphogenesis in zebrafish embryos using robot-assisted tissue micromanipulation," *Nature Commun.*, vol. 13, no. 1, 2022, Art. no. 7934.

[11] F. Xiong, W. Ma, B. Bénazéraf, L. Mahadevan, and O. Pourquié, "Mechanical coupling coordinates the co-elongation of axial and paraxial tissues in avian embryos," *Devlop. Cell*, vol. 55, no. 3, pp. 354–366, 2020.
[12] L. Thomson, L. Muresan, and B. Steventon, "The zebrafish presomitic mesoderm elongates through compaction-extension," *Cells Develop.*, vol. 168, 2021, Art. no. 203748.
[13] S. B. P. McLaren and B. J. Steventon, "Anterior expansion and posterior addition to the notochord mechanically coordinate zebrafish embryo axis elongation," *Development*, vol. 148, no. 18, 2021, Art. no. dev199459.
[14] Y. Zhang, B. K. Chen, X. Liu, and Y. Sun, "Autonomous robotic pick-and-place of microobjects," *IEEE Trans. Robot.*, vol. 26, no. 1, pp. 200–207, Feb. 2010.
[15] Y. Sun and B. J. Nelson, "Biological cell injection using an autonomous microrobotic system," *Int. J. Robot. Res.*, vol. 21, no. 10/11, pp. 861–868, 2002.
[16] Z. Zhang, X. Wang, J. Liu, C. Dai, and Y. Sun, "Robotic micromanipulation: Fundamentals and applications," *Annu. Rev. Control Robot. Auton. Syst.*, vol. 2, no. 1, pp. 181–203, 2019.
[17] Z. Gong, B. K. Chen, J. Liu, and Y. Sun, "Robotic probing of nanostructures inside scanning electron microscopy," *IEEE Trans. Robot.*, vol. 30, no. 3, pp. 758–765, Jun. 2014.
[18] I. Holland and J. A. Davies, "Automation in the life science research laboratory," *Front. Bioeng. Biotechnol.*, vol. 8, 2020, Art. no. 571777.
[19] J. Liu et al., "Automated vitrification of embryos: A robotics approach," *IEEE Robot. Automat. Mag.*, vol. 22, no. 2, pp. 33–40, Jun. 2015.
[20] C. Dai et al., "Design and control of a piezo drill for robotic piezo-driven cell penetration," *IEEE Robot. Automat. Lett.*, vol. 5, no. 2, pp. 339–345, Apr. 2020.
[21] L. Ghanbari et al., "Craniobot: A computer numerical controlled robot for cranial microsurgeries," *Sci. Rep.*, vol. 9, 2019, Art. no. 1023.
[22] I. I. Iordachita, M. D. De Smet, G. Naus, M. Mitsuishi, and C. N. Riviere, "Robotic assistance for intraocular microsurgery: Challenges and perspectives," *Proc. IEEE*, vol. 110, no. 7, pp. 893–908, Jul. 2022.
[23] M. Nambi, P. S. Bernstein, and J. J. Abbott, "A compact telemanipulated retinal-surgery system that uses commercially available instruments with a quick-change adapter," *J. Med. Robot. Res.*, vol. 1, no. 02, 2016, Art. no. 1630001.
[24] N. Wang, X. Zhang, M. Li, H. Zhang, D. Stoyanov, and A. Stilli, "A 5-DOFs robot for posterior segment eye microsurgery," *IEEE Robot. Automat. Lett.*, vol. 7, no. 4, pp. 10128–10135, Oct. 2022.
[25] A. B. Webb et al., "Persistence, period and precision of autonomous cellular oscillators from the zebrafish segmentation clock," *eLife*, vol. 5, 2016, Art. no. e08438.
[26] C. Schröter, L. Herrgen, A. Cardona, G. J. Brouhard, B. Feldman, and A. C. Oates, "Dynamics of zebrafish somitogenesis," *Devlop. Dyn.*, vol. 237, no. 3, pp. 545–553, 2008.
[27] O. Ronneberger, P. Fischer, and T. Brox, "U-Net: Convolutional networks for biomedical image segmentation," in *Proc. Int. Conf. Med. Image Comput. Comput.-Assist. Interv.*, 2015, pp. 234–241.
[28] Z. Alom, M. Hasan, C. Yakopcic, T. M. Taha, and V. K. Asari, "Recurrent residual convolutional neural network based on U-Net (R2U-Net) for medical image segmentation," 2018, *arXiv:1802.06955*.
[29] C. Aztekin, T. W. Hiscock, J. C. Marioni, J. B. Gurdon, B. D. Simons, and J. Jullien, "Identification of a regeneration-organizing cell in the Xenopus tail," *Science*, vol. 364, no. 6441, pp. 653–658, 2019.
[30] C. Aztekin et al., "The myeloid lineage is required for the emergence of a regeneration-permissive environment following *xenopus* tail amputation," *Development*, vol. 147, no. 3, 2020, Art. no. dev185496.
[31] E. Mailand et al., "Tissue engineering with mechanically induced solid-fluid transitions," *Adv. Mater.*, vol. 34, no. 2, 2022, Art. no. 2106149.
[32] D. Čapek et al., "EmbryoNet: Using deep learning to link embryonic phenotypes to signaling pathways," *Nature Methods*, vol. 20, pp. 815–823, 2023.